Structural, Stabilities, and Electronic Properties of Bimetallic Mg_2-doped Silicon Clusters

Shuai Zhang[a], Zhi-Peng Wang[a], Cheng Lu[a,b], Chong Wang[a], Gen-Quan Li[a], and Zhi-Wen Lu[a]

[a] Department of Physics, Nanyang Normal University, Nanyang 473061, China
[b] State Key Laboratory of Superhard Materials, Jilin University, Changchun 130012, China

Reprint requests to C. L.; E-mail: lucheng@calypso.cn

Z. Naturforsch. **69a**, 481 – 488 (2014) / DOI: 10.5560/ZNA.2014-0043
Received March 5, 2014 / revised April 19, 2014 / published online July 16, 2014

The equilibrium geometries, relative stabilities, growth patterns, and electronic properties of magnesium-doped silicon clusters Mg_2Si_n ($n = 1-11$) have been systematically investigated at the B3LYP/6-311G (d) level. A large number of initial configurations are optimized and the lowest-energy stable geometries of Mg_2Si_n ($n = 1-11$) clusters with different spin multiplicities are determined. The results indicate that the most stable configurations for Mg_2Si_n clusters favor the three-dimensional structures at $n = 3-11$. The analyses of the averaged binding energies, fragmentation energies, second-order energy difference, and HOMO–LUMO gaps suggest that the Mg_2Si_4 and Mg_2Si_6 clusters have the stronger relative stability, and magnesium atoms doping enhances the chemical activity of the silicon framework. The natural population and natural electronic configuration analyses show that the charge transfer occurs from the $3s$ orbital of the magnesium atoms to the silicon atoms and $3p$ orbital of the magnesium atoms.

Key words: Mg_2Si_n Clusters; Density Functional Theory; Geometrical Structures; Electronic Properties.

1. Introduction

Alkaline-earth metal silicides have been the subject of considerable interest for several decades, not only because they provide a model system for the detailed study of silicon-based microelectronics, but because of the undeniable importance of silicon in the semiconductor industry [1 – 3]. They have unusual physical and chemical properties, such as low resistivity, high elevated temperature strength, high specific strength, high elastic modulus, and low thermal conductivity, and wide applications in many fields, which include the usage in the aviation and automobile industries. However, there is little known about the molecular level mechanism, partly due to the difficulty in studying, both theoretically and experimentally, a typically solid–solid reaction on the molecular scale. Small clusters offer a new way in studying such systems, which can provide insight into the strength and nature of the metal–silicon bonds [4 – 9]. Beck [10] reported the observation of a reaction between a metal atom and silicon in a supersonic jet to form metal atom–silicon clusters. Based on the anion photoelectron spectroscopy, Grubisic et al. [11] investigated several $LnSi_n$ cluster anion systems (Ln=Yb, Eu, Sm, Gd, Ho, Pr), which expands the range of studied lanthanide–silicon systems to encompass half of the lanthanide series. Kishi et al. [12] performed the photoelectron spectroscopy measurements on the silicon–sodium cluster anions. The ionization energy and electron affinities of Si_nNa_m revealed several patterns with the number of the sodium atoms, and the charge transfer mechanism in the cluster reflects the nature of the electron-accepting orbitals of the corresponding Si_n and the adsorption types of the sodium atoms. To explore the structural evolution of chromium-doped silicon clusters, Kong et al. [13] investigated $CrSi_n^-$ ($n = 3-12$) clusters using the anion photoelectron spectroscopy and density functional theory (DFT) calculations. The combination of experimental measurement and theoretical calculations suggested that the onset of endohedral structure in $CrSi_n^-$ clusters occurs at $n = 10$, and the magnetic properties of the $CrSi_n^-$ clusters are correlated with their

geometric structures. By using first-principles DFT-generalized gradient approximation (GGA) calculations, Guo et al. [14] reported the stabilities and magnetic properties of the transition metal encapsulated MSi_n (M=Sc, Ti, V, Cr, Mn, Fe, Co, Ni, Cu, Zn; $n = 8-16$) clusters.

Although silicon clusters doped with many different metals have been studied extensively in recent years, there are no systematic theoretical and experimental investigations on Mg_2Si_n clusters. To gain insight into the geometries and electronic properties of the Mg_2Si_n clusters and further enrich our knowledge of silicon-based clusters, we carried out the computational studies on a series of Mg_2Si_n ($n = 1-11$) clusters. We hope that the theoretical study will be useful to understand the geometric structures of Mg_2Si_n ($n = 1-11$) clusters in the ground state and can provide useful information in exploring the physical mechanism of the growth behaviors of Mg_2Si_n clusters.

2. Computational Methods

All geometrical structure optimization and frequency analysis of Mg_2Si_n ($n = 1-11$) clusters are performed by using DFT with 6-311G (d) basis set, as implemented in the Gaussian 09 program package [15]. The B3LYP exchange-correlation potential [16, 17] is used. To gain the lowest-energy structures, a great deal of initial configurations of Mg_2Si_n clusters, which include one-dimensional (1D), two-dimensional (2D), and three-dimensional (3D) configurations, are sought using the following two approaches:

(i) by considering the numbers of previous reported Si_n, XSi_n, and X_2Si_n structures [18–23];
(ii) by placing magnesium atoms at various adsorption or substitutional sites on the basis of optimized Si_n, XSi_n or X_2Si_n geometries, i. e., Mg-capped, Mg-substituted, and Mg-encapsulated patterns.

Due to the spin polarization, all configurations are optimized at possible spin multiplicities (singlet, triplet, and quintet) [24]. To ensure the reliability of theoretical method and basis set used here, the bond length, vibrational frequency, vertical ionization potential (VIP), and vertical electron affinity (VEA) [24] of Si_2, Mg_2, and MgSi dimers are calculated and illustrated in Table 1. For the Si_2 dimer, the calculated values are $r(Si_2) = 2.17$ Å, $\omega(Si_2) = 540.37\ cm^{-1}$, $VIP(Si_2) = 9.13$ eV, and $VEA(Si_2) = 2.00$ eV, which are in good agreement with the available experimental results [25–27]. For the Mg_2 dimer, the theoretical results of bond length (3.93 Å) and vibrational frequency ($44.91\ cm^{-1}$) are also in good agreement with the experimental results [28]. So, the theoretical method and basis set are reasonable.

3. Results and Discussion

3.1. Geometrical Structures

For Mg_2Si_n ($n = 1-11$) clusters, we have explored a lot of low-lying isomers and determined the lowest-energy isomers. Although many initial structures have been taken into account, only the obtained ground state and some metastable isomers are plotted in Figure 1. According to their energies from low to high, these isomers are designated by *n*a, *n*b, *n*c, and *n*d, where *n* represents the number of silicon atoms in the Mg_2Si_n clusters.

The lowest-energy structure of Mg_2Si (1a) is a triplet with C_{2v} symmetry and the Mg–Si–Mg apex angle is 72.21°, in which the two magnesium atoms are located on the two sides. The linear isomer Si–Mg–Mg 1b ($C_{\infty v}$) with the silicon atom at one end is 0.47 eV higher in energy than the 1a isomer. All possible initial structures of Mg_2Si_2 clusters with different spin

Table 1. Comparison of the calculated properties for Si_2, Mg_2, and MgSi dimers with the corresponding available experimental data.

	Si_2		Mg_2		MgSi	
	Cal	Expt	Cal	Expt	Cal	Expt
r (Å)	2.17	2.246[a]	3.93	3.89[d]	2.58	–
ω (cm^{-1})	540.37	511.0[a]	44.91	45[d]	288.33	–
VIP (eV)	9.13	> 8.49[b]	6.59	–	6.82	–
VEA (eV)	2.00	2.176 ± 0.002[c]	0.04	–	0.59	–

[a][25], [b][26], [c][27], [d][28]

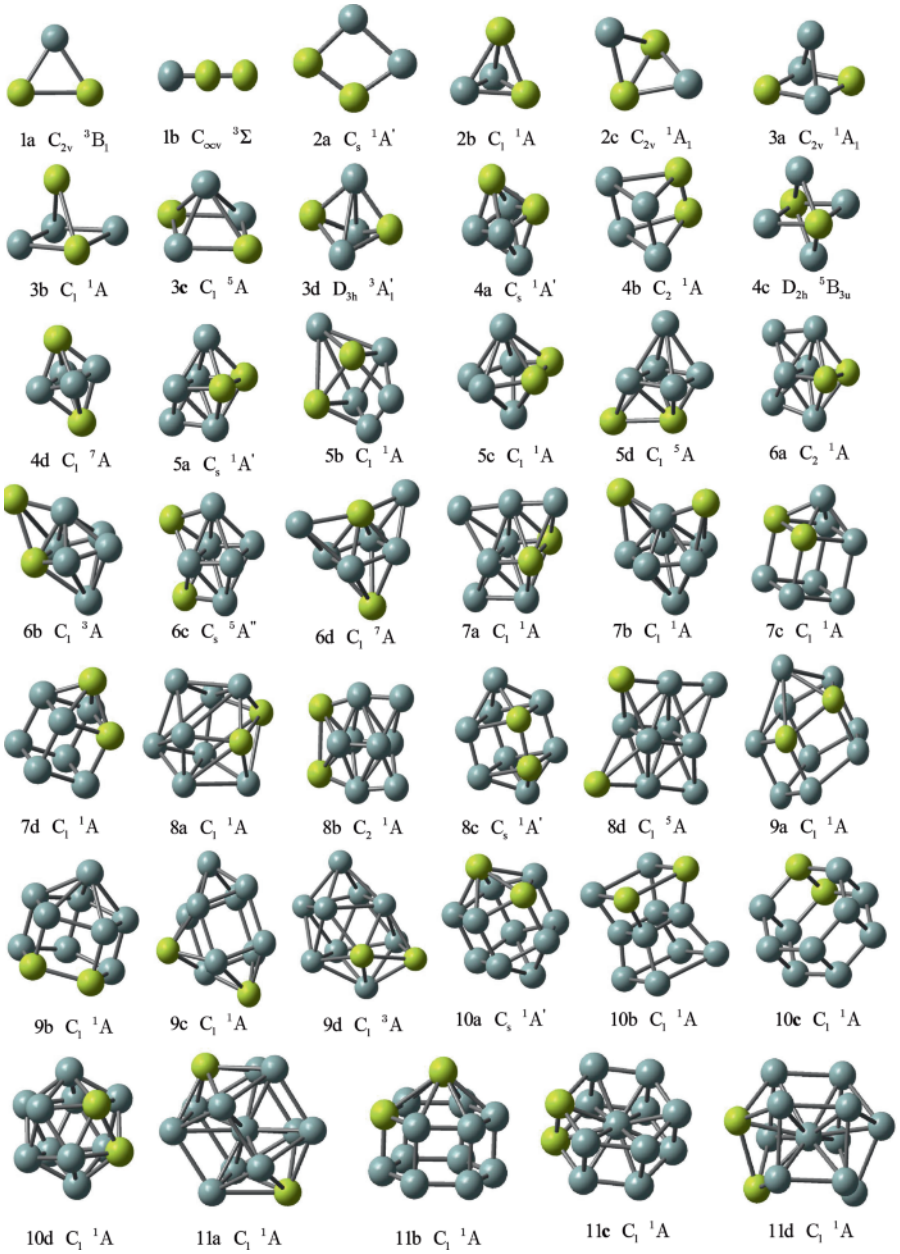

Fig. 1 (colour online). Lowest-energy and low-lying structures of Mg_2Si_n ($n = 1-11$) clusters.

multiplicities are optimized. The calculated results reveal that the ground state isomer 2a is a rhombus-like structure with singlet state $^1A'$, which can be viewed as a planar rhombus lowest-energy structure of Si_4 [18] by replacing two silicon atoms with magnesium atoms. The pyramid isomer 2b with ^1A electronic state is 0.10 eV higher in energy than the 2a isomer. The third isomer 2c with C_{2v} symmetry is a butterfly structure with the Mg–Mg bond for the 'body' of the insect plus four Mg–Si bonds at the edges of the 'wings', and its energy is higher than that of isomer 2b by 0.54 eV. With regard to the Mg_2Si_3 cluster, the lowest-energy isomer 3a is a pyramid structure with C_{2v} symmetry, which can be described as a substituted version of the

structure of the ground state Si_5 [18] cluster. The low-lying isomers 3b and 3c are similar to the 3a isomer, the difference between them is the site of magnesium atom, but the energy of the 3a isomer is lower than that of 3b and 3c isomers by 0.65 and 0.77 eV, respectively. From $n = 3$ afterwards, the 3D structures show higher stability than the planar structures. Among the isomers of Mg_2Si_4, the tetragonal bipyramid 4a with C_s symmetry is found to be the most stable isomer, which is in agreement with the results for $V_2Si_4^-$ [29]. The isomer 4b with C_2 symmetry is a triangular prism structure, and its energy is 0.20 eV higher than that of the 4a isomer. Other low-lying isomers (4c and 4d), which have the structure similar to the 4a isomer, are higher in total energy than the lowest-energy isomer 4a by 0.74 and 0.83 eV, respectively. At $n = 5$, the isomers 5a and 5d are two structures derived from the low-lying isomers of Mg_2Si_4 clusters, where the fifth silicon or magnesium atom is added into the Mg_2Si_4 clusters at different site. The optimized results indicate that the isomer 5a with *Cs* symmetry is the ground state structure. When the 4b isomer is capped with one silicon atom, the metastable isomer 5b (C_1) is generated, which has an energy higher than isomer 5a by 0.10 eV. The isomer 5c (C_1) is a pentagonal bipyramid, and its energy is higher than that of the 5b isomer by 0.01 eV.

For Mg_2Si_6 clusters, a lot of possible configurations and spin states are tried to identify the ground state. The isomer 6a (C_2) is evaluated to be the ground state structure, which can be regarded as capping one silicon atom on the lowest-energy isomer 5a. The geometry of isomer 6b (C_1) can be created from the metastable isomer 5c by capping one magnesium atom. The isomer 6c (C_s) has a structure similar to the isomer 6a, the difference between them is the site of the magnesium atom. The metastable isomer 6d (C_1) is formed by capping two silicon atoms on the metastable isomer 4d. The energy of 6a is lower than those of 6b, 6c, and 6d isomers by 0.48, 0.63, and 0.81 eV, respectively. According to the calculated total energies of the four Mg_2Si_7 isomers, the isomer 7a with C_1 symmetry is proved to be the ground state structure among all the isomers. The metastable isomer 7b (C_1) can be viewed as capping one atom on the metastable isomer 6b. The other isomers (Fig. 1 (7c,C_1), (7d,C_1)) have lower stability than the 7b isomer, and their energies are higher than that of the 7b isomer by 0.13 and 0.49 eV, respectively.

At $n = 8$, four kinds of structures can be verified to be the minima. The isomer 8a with C_1 symmetry is predicted to be the lowest-energy structure. The isomer 8b (C_2) is obtained when the 7a isomer is capped with one silicon atom. And its energy is higher than that of the 8a isomer by 0.14 eV. Other isomers, such as Figure 1 (8c, C_s) and (8d, C_1) are 0.60 and 0.85 eV higher in energy than that of the ground state isomer 8a, respectively. The low energy isomers for Mg_2Si_9 are plotted in Figure 1 (9a – 9d). When one silicon atom is bicapped on the top of the pentagonal prism, the lowest-energy isomer 9a is obtained. The other low-lying isomers 9b, 9c, and 9d are 0.01, 0.10, and 0.88 eV higher in energy than that of the ground state, respectively. For $n = 10$, we found that isomer 10a which is generated after one silicon atom is capped on the top of lowest-energy isomer 9a, is optimized to be the ground state structure. The isomer 10b with C_1 symmetry is a 4-4-4 layer structure, which is expected to be the lowest-energy structure. However, its energy is higher than that of isomer 10a by 0.17 eV. The other isomers 10c (C_1) and 10d (C_1) have weaker stability than 10a because their energies are higher than that of the 10a isomer by 0.51 and 0.73 eV, respectively. Likewise, we identified four low energy isomers for Mg_2Si_{11}, as shown in Figure 1. The calculations turn out that the Si-centered cage-like geometry 11a is the lowest-energy structure in all isomers. The other low-lying isomers, including Figure 1 (11b, C_1), (11c, C_1), and (11d, C_1), which are 0.04, 0.77, and 0.81 eV higher in energy than that of the 11a isomer, respectively.

According to the above results, the lowest-energy geometries of Mg_2Si_n clusters are found to adopt 3D forms for $n = 3 – 11$ and 2D structures for $n = 1 – 2$. In addition, the Mg_2Si_{n-1} structure capped with one magnesium or silicon atom is the dominant growth pattern for Mg_2Si_n clusters of various sizes ($n = 1 – 11$).

3.2. Relative Stabilities

To predict the relative stabilities of the lowest-energy Mg_2Si_n ($n = 1 – 11$) clusters, we calculated the averaged binding energies [$E_b(n)$], fragmentation energy [$E_f(n)$], and second-order energy difference [$\Delta_2 E(n)$] and summarized the theoretical results in Table 2. The $E_b(n)$, $E_f(n)$, and $\Delta_2 E(n)$ for Mg_2Si_n clusters can be expressed by the following formulas [30, 31]:

Table 2. Calculated averaged binding energies (E_b), the second-order energy difference ($\Delta_2 E$), the fragmentation energy (E_f), HOMO–LUMO energy gaps (E_{gap}), and Frequencies of the lowest- energy structures for Mg_2Si_n ($n = 1-11$) clusters.

n	E_b (eV)	$\Delta_2 E$ (eV)	E_f (eV)	E_{gap} (eV)	Frequency (cm^{-1})
1	0.53			1.51	120.1, 226.2, 293.3
2	1.19	−0.10	3.17	1.42	42.6, 126.2, 185.4, 193.1, 320.8, 516.3
3	1.79	−1.14	3.27	1.55	61.5, 110.4, 142.3, 198.2, 232.3, 303.1
4	2.07	3.33	4.41	2.37	70.4, 77.5, 158.0, 237.6, 279.7, 286.3
5	2.22	−0.74	3.08	1.75	72.4, 72.9, 134.9, 144.8, 149.2, 197.9
6	2.42	0.74	3.82	2.58	53.4, 55.6, 80.9, 124.2, 145.9, 165.6
7	2.49	−0.64	3.08	2.23	56.9, 83.0, 116.1, 135.1, 164.6, 167.8
8	2.61	0.68	3.72	2.56	65.2, 76.6, 95.8, 100.5, 125.1, 128.6
9	2.65	−0.13	3.05	2.43	58.2, 75.7, 93.4, 118.8, 124.4, 140.6
10	2.70	0.17	3.18	1.85	63.3, 84.1, 113.3, 116.9, 127.4, 139.2
11	2.72		3.00	1.84	68.4, 82.7, 106.4, 119.3, 123.4, 133.1

$$E_b(n) = \frac{nE_k(\mathrm{Si}) + 2E_k(\mathrm{Mg}) - E_k(\mathrm{Mg_2Si}_n)}{n+2}, \quad (1)$$

$$E_f(n) = E_k(\mathrm{Mg_2Si}_{n-1}) + E_k(\mathrm{Si}) - E_k(\mathrm{Mg_2Si}_n), \quad (2)$$

$$\Delta_2 E(n) = E_k(\mathrm{Mg_2Si}_{n+1}) + E_k(\mathrm{Mg_2Si}_{n-1}) - 2E_k(\mathrm{Mg_2Si}_n), \quad (3)$$

where E_k represents the total energy of the lowest-energy silicon atom, magnesium atom, Mg_2Si_n cluster, Mg_2Si_{n-1} cluster, and Mg_2Si_{n+1} cluster, respectively.

The $E_b(n)$, $E_f(n)$, and $\Delta_2 E(n)$ values of the most stable Mg_2Si_n clusters at the B3LYP/6-311G (d) level of theory as a function of clusters size are depicted in Figure 2a and b. As shown in Figure 2, with the increasing size of clusters, the $E_b(n)$ of Si_{n+2} [20] and Mg_2Si_n clusters gradually increase. When $n \leq 3$, the $E_b(n)$ rapidly increase as the cluster size of the pure Si_{n+2} and Mg_2Si_n clusters increase, then the $E_b(n)$ of the pure Si_{n+2} and Mg_2Si_n clusters increases smoothly as the cluster size grows for $n > 3$. The results imply that Si_{n+2} and Mg_2Si_n clusters continuously gain energy during the growth. The $E_b(n)$ increases rapidly from Mg_2Si (0.53 eV) to Mg_2Si_3 (1.79 eV), corresponding to the structure transition from two to three dimensions. In addition, the $E_b(n)$ of Mg_2Si_n doped counterparts is obviously smaller than that of the corresponding pure Si_{n+2} [20] cluster, which hints that the impurity magnesium atoms can enhance the chemical activity of the pure silicon clusters. This phenomenon is similar to the $E_b(n)$ of Cu_2Si_n clusters [32]. The fragmentation energy $E_f(n)$ and second-order energy difference $\Delta_2 E(n)$ are sensitive indicators of the relative stability. Three prominent maxima $E_f(n)$ for the most stable Mg_2Si_n clusters are found at $n = 4$, 6, and 8, indicating that the lowest-energy Mg_2Si_4, Mg_2Si_6, and Mg_2Si_8 clusters have stronger relative stabilities compared to their corresponding neighbors. It is also found that the $\Delta_2 E(n)$ for the Mg_2Si_n clusters is bigger than other neighboring clusters when $n = 2$, 4, 6 and 8, indicating these clusters possess higher relative stabilities. This result is well consistent with the maxima presented in the fragmentation energy $E_f(n)$.

3.3. HOMO–LUMO Gaps and Charge Transfer

The energy gaps E_{gap} (The highest occupied-lowest unoccupied molecular orbital (HOMO–LUMO) energy gap) reflects the ability of electrons to jump from an occupied orbital to an unoccupied orbital, and represents the ability for the molecular to participate in the chemical reactions to some degree [33]. It is found that a larger gap associates with higher stability, in other words, a bigger gap signifies a weaker chemical activity. The E_{gap} for the lowest-energy geometry on the pure Si_{n+2} [20] and doped Mg_2Si_n ($n = 1-11$) clusters against the cluster size are plotted in Figure 2c. The data in Figure 2c show that the Mg_2Si_n clusters with $n = 1$, 4, 6, and 9 exhibit relatively wider E_{gap}, suggesting that these clusters are more stable than their neighbors, which is in agreement with the behavior of the fragment energy $E_f(n)$ and second-order difference energy $\Delta_2 E(n)$ (except for $n = 1$ and 9) shown in Figure 2a and b, respectively. So it can be concluded that the magic clusters are found at $n = 4$ and 6 for the Mg_2Si_n clusters, reflecting that the Mg_2Si_4 and Mg_2Si_6 are the most stable geometries. Particularlly, the Mg_2Si_6 cluster has the largest E_{gap} of 2.58 eV compared with others, including the Mg_2Si_4 cluster. Moreover, Figure 2c shows that the E_{gap} of the pure Si_{n+2} clusters are larger than those of the Mg_2Si_n clus-

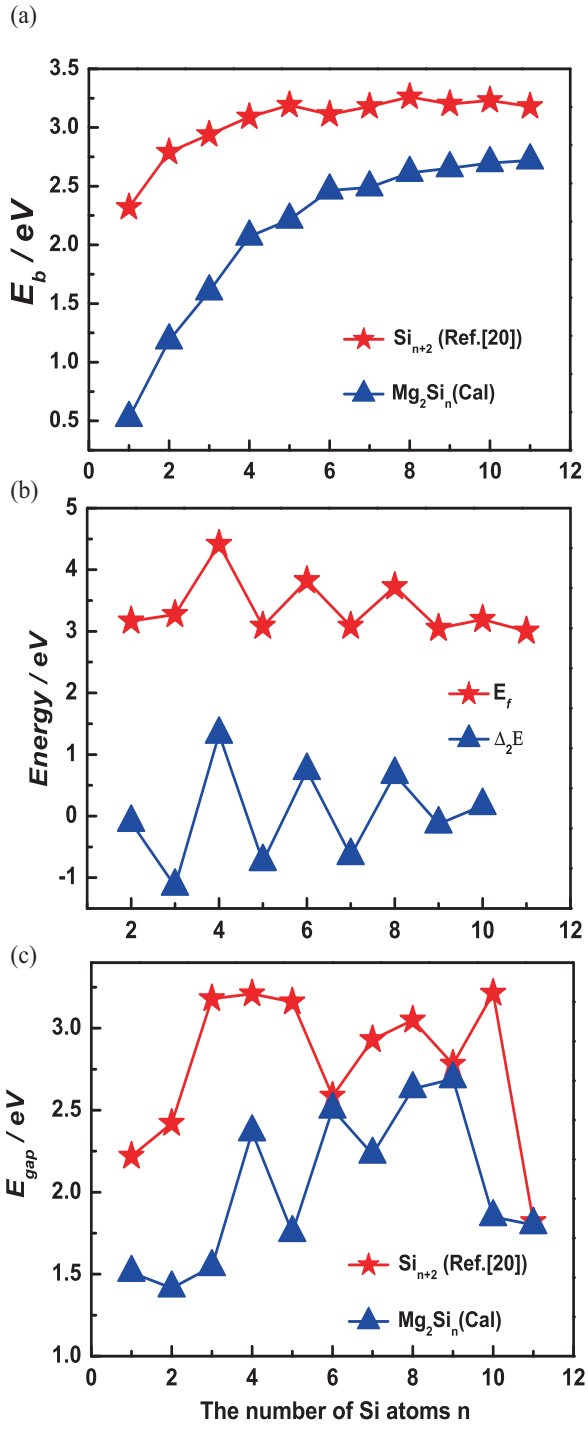

Fig. 2 (colour online). Size dependence of the averaged binding energy E_b, second-order difference energy $\Delta_2 E$, fragment energy E_f, and the HOMO–LUMO energy gap E_{gap} of the lowest-energy structures for Mg_2Si_n ($n = 1-11$) clusters.

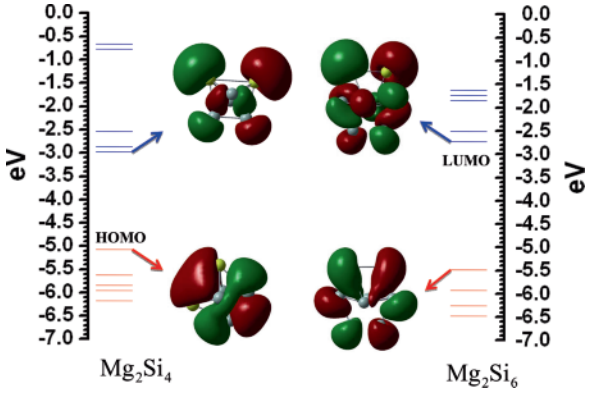

Fig. 3 (colour online). Calculated molecular orbital energy levels of Mg_2Si_4 and Mg_2Si_6 clusters together with the molecular orbital maps of the HOMOs and LUMOs.

ters, which means that the metallic characteristics of Mg_2Si_n clusters are enhanced by the doping of Mg atoms.

In order to investigate the effect of magnesium atoms doping on electronic structure of silicon cluster, the molecular orbital energy levels of the magic clusters for Mg_2Si_n clusters are calculated and displayed in Figure 3. The red line (lower half of the ordinate) shows the occupied orbital and the blue line (upper half of the ordinate) shows the unoccupied orbital. Compared with Mg_2Si_4 and Mg_2Si_6, Mg_2Si_6 is obviously characteristic of the molecular orbital producing the degeneration of the energy level in the vicinity of the HOMO–LUMO, and the energy level of the LUMO elevated strongly, which probably leads to its largest value of energy gap.

The natural population analysis (NPA) can provide reliable charge transfer information. So, the NPA analysis of magnesium atoms for the lowest-energy Mg_2Si_n clusters are calculated and listed in Table 3. From the table, one can see that the sign of the charges on magnesium atoms (0.388 – 0.861) is positive, while most of the silicon atoms possess negative charges. This result indicates that the charges transfer from the magnesium atoms to the Si_n frame, that is, silicon atoms act as electron acceptor in all Mg_2Si_n clusters. This may be caused by reason that the electronegativity of magnesium (1.31) is much smaller than that of silicon (1.90) [34]; therefore, magnesium has a stronger ability to lose electrons.

Moreover, to understand the internal charge transfer, the natural electron configurations (NEC) of the mag-

Table 3. Natural population analysis (NPA) of magnesium atoms in the lowest-energy structures of Mg_2Si_n ($n = 1-11$) clusters.

	1	2	3	4	5	6	7	8	9	10	11
Mg (1)	0.388	0.546	0.725	0.689	0.505	0.513	0.776	0.783	0.587	0.680	0.861
Mg (2)	0.388	0.372	0.725	0.689	0.505	0.513	0.776	0.783	0.405	0.843	0.747

Table 4. Charges of $3s$, $3p$, $4s$, $3d$, and $4p$ orbitals for the magnesium atoms in Mg_2Si_n ($n = 1-11$) clusters.

		1	2	3	4	5	6	7	8	9	10	11
	$3s$	1.34	0.75	0.86	0.85	1.01	1.14	0.62	0.87	1.14	0.52	0.66
	$3p$	0.26	0.68	0.39	0.44	0.47	0.33	0.56	0.32	0.25	0.75	0.46
Mg (1)	$4s$	0.01		0.01							0.01	
	$3d$	0.01	0.01	0.01	0.01	0.01	0.01	0.02	0.01	0.01	0.03	0.01
	$4p$	0.01	0.01	0.01	0.01	0.01	0.01	0.02	0.01	0.01	0.02	0.01
	$3s$	1.34	1.40	0.86	0.85	1.01	1.14	0.62	0.87	0.96	0.75	0.83
	$3p$	0.26	0.22	0.39	0.44	0.47	0.33	0.56	0.32	0.61	0.44	0.40
Mg (2)	$4s$	0.01		0.01						0.01	0.01	0.01
	$3d$	0.01		0.01	0.01	0.01	0.01	0.02	0.01			
	$4p$	0.01		0.01	0.01	0.01	0.01	0.02	0.01			

nesium atoms in the lowest-energy Mg_2Si_n ($n = 1-11$) clusters are calculated and summarized in Table 4. For a free magnesium atom, the configuration of valence electrons is $3s^2$. With regard to the impurities, the NEC values reveal that the $3s$ orbital loses $0.60-1.38$ electrons, while the $3p$ orbital receives $0.22-0.75$ electrons for Mg_2Si_n clusters. The contribution of the $4s$, $3d$, and $4p$ orbitals are nearly zero, so it can be neglected. Therefore, we can conclude that the charges in the lowest-energy Mg_2Si_n clusters transfer from the $3s$ orbital of the magnesium atom to the silicon atoms and $3p$ orbital of the magnesium atom. And the electronic charge distributions of Mg_2Si_n clusters are primarily governed by s- and p-orbital interactions. While the charges of $3s$ and $3p$ orbitals for two magnesium atoms in the lowest-energy Mg_2Si_n clusters are equal except for the $Mg_2Si_{2,9-11}$ clusters.

4. Conclusion

The equilibrium geometries, growth pattern behaviors, relative stabilities, and electronic properties of magnesium-doped silicon clusters have been obtained by using density functional theory at the B3LYP/6-311G (d) level. In this work, we focused on analyzing a series of properties for these Mg_2Si_n clusters including averaged binding energies, fragmentation energy, second-order energy difference, and HOMO–LUMO energy gaps. The theoretical results show that the Mg_2Si_4 and Mg_2Si_6 are the most stable geometries in Mg_2Si_n ($n = 1-11$) clusters. By analyzing the natural population and natural electronic configuration, it is find that the charges transfer from $3s$ orbital of the magnesium atom to the silicon atoms and $3p$ orbital of the magnesium atom, namely magnesium atoms act as electron donors in all Mg_2Si_n clusters.

Acknowledgements

This work is supported by the Natural Science Foundation of China (Nos. 11304167 and 51374132), Postdoctoral Science Foundation of China (No. 20110491317), Open Project of State Key Laboratory of Superhard Materials in Jilin University (No. 201405), Young Core Instructor Foundation of Henan Province (No. 2012GGJS-152), and Natural Science Foundation of Nanyang Normal University (No. zx20100011).

[1] M. Baba, K. Ito, W. J. Du, T. Sanai, K. Okamoto, K. Toko, S. Ueda, Y. Imai, A. Kimura, and T. Suemasu, J. Appl. Phys. **114**, 123702 (2013).

[2] Y. Imai, Y. Mori, S. Nakamura, and K. Takarabe, J. Alloys. Compd. **558**, 179 (2013).

[3] J. P. Chou, H. Y. T. Chen, C. R. Hsing, C. M. Chang, C. Cheng, and C. M. Wei, Phys. Rev. B **80**, 165412 (2009).

[4] L. Q. Zhang, Y. Cheng, Z. W. Niu, and G. F. Ji, Z. Naturforsch. **69a**, 52 (2014).

[5] Ş. Şenentürk, and Y. Ekincioğlu, Z. Naturforsch. **67a**, 289 (2012).
[6] P. Claes, E. Janssens, V. T. Ngan, P. Gruene, J. T. Lyon, D. J. Harding, A. Fielicke, M. T. Nguyen, and P. Lievens, Phys. Rev. Lett. **107**, 173401 (2011).
[7] X. Y. Kong, X. J. Deng, H. G. Xu, Z. Yang, X. L. Xu, and W. J. Zheng, J. Chem. Phys. **138**, 244312 (2013).
[8] P. Claes, V. T. Ngan, M. Haertelt, J. T. Lyon, A. Fielicke, M. T. Nguyen, P. Lievens, and E. Janssens, J. Chem. Phys. **138**, 194301 (2013).
[9] Z. J. Zhou and Y. F. Hu, Z. Naturforsch. **67a**, 99 (2012).
[10] S. M. Beck, J. Chem. Phys. **90**, 6306 (1989).
[11] A. Grubisic, Y. J. Ko, H. P. Wang, and K. H. Bowen, J. Am. Chem. Soc. **131**, 10783 (2009).
[12] R. Kishi, H. Kawamata, and Y. Negishi, J. Chem. Phys. **107**, 10029 (1997).
[13] X. Y. Kong, H. G. Xu, and W. J. Zheng, J. Chem. Phys. **137**, 64307 (2012).
[14] L. J. Guo, G. F. Zhao, Y. Z. Gu, X. Liu, and Z. Zeng, Phys. Rev. B **77**, 195417 (2008).
[15] M. J. Frisch, G. W. Trucks, H. B. Schlegel, G. E. Scuseria, M. A. Robb, J. R. Cheeseman, J. A. Montgomery Jr, T. Vreven, K. N. Kudin, J. C. Burant, J. M. Millam, S. S. Iyengar, J. Tomasi, V. Barone, B. Mennucci, M. Cossi, G. Scalmani, N. Rega, G. A. Petersson, H. Nakatsuji, M. Hada, M. Ehara, K. Toyota, R. Fukuda, J. Hasegawa, M. Ishida, T. Nakajima, Y. Honda, O. Kitao, H. Nakai, M. Klene, X. Li, J. E. Knox, H. P. Hratchian, J. B. Cross, V. Bakken, C. Adamo, J. Jaramillo, R. Gomperts, R. E. Stratmann, O. Yazyev, A. J. Austin, R. Cammi, C. Pomelli, J. Ochterski, P. Y. Ayala, K. Morokuma, G. A. Voth, P. Salvador, J. J. Dannenberg, V. G. Zakrzewski, S. Dapprich, A. D. Daniels, M. C. Strain, O. Farkas, D. K. Malick, A. D. Rabuck, K. Raghavachari, J. B. Foresman, J. V. Ortiz, Q. Cui, A. G. Baboul, S. Clifford, J. Cioslowski, B. B. Stefanov, G. Liu, A. Liashenko, P. Piskorz, I. Komaromi, R. L. Martin, D. J. Fox, T. Keith, M. A. Al-Laham, C. Y. Peng, A. Nanayakkara, M. Challacombe, P. M. W. Gill, B. G. Johnson, W. Chen, M. W. Wong, C. Gonzalez, and J. A. Pople, Gaussian 09 Rev C.01, Gaussian Inc., Pittsburgh, PA, 2009.
[16] A. D. Becke, Phys. Rev. A **38**, 3098 (1988).
[17] C. Lee, W. Yang, and R. G. Parr, Phys. Rev. B **37**, 785 (1988).
[18] C. Pouchan and D. Bégue, J. Chem. Phys. **121**, 4628 (2004).
[19] H. G. Xu, Z. G. Zhang, Y. Feng, and W. J. Zheng, Chem. Phys. Lett. **498**, 22 (2010).
[20] W. Qin, W. C. Lu, L. Z. Zhao, Q. J. Zang, C. Z. Wang, and K. M. Ho, J. Phys. Cond. Mat. **21**, 455501 (2009).
[21] R. Robles and S. N. Khanna, J. Chem. Phys. **130**, 164313 (2009).
[22] J. G. Han, R. N. Zhao, and Y. H. Duan, J. Phys. Chem. A **111**, 2148 (2007).
[23] J. Z. Ye and B. X. Li, Physica B **405**, 1461 (2010).
[24] Y. R. Zhao, X. Y. Kuang, B. B. Zheng, Y. F. Li, and S. J. Wang, J. Phys. Chem. A **115**, 569 (2011).
[25] K. P. Huber and G. Herzberg, Constants of Diatomic Molecules, Van Nostrand / Reinhold, New York 1979.
[26] W. A. de Heer, W. D. Knight, M. Y. Chou, and M. L. Cohen, Solid State Phys. Vol. 40, Acadmic, San Diego 1987.
[27] T. N. Kitsopoulos, C. J. Chick, Y. Zhao, and D. M. Neumark, J. Chem. Phys. **95**, 1441 (1991).
[28] F. Ruette, M. Sánchez, R. Anez, A. Bermúdez and A. Sierraalta, J. Mol. Struct: Theochem. **729**, 19 (2005).
[29] H. G. Xu, Z. G. Zhang, Y. Feng, J. Y. Yuan, Y. C. Zhao, and W. J. Zheng, Chem. Phys. Lett. **487**, 204 (2010).
[30] D. Die, X. Y. Kuang, J. J. Guo, and B. X. Zhang, J. Phys. Chem. Solids. **71**, 770 (2010).
[31] Y. F. Li, A. J. Mao, Y. Li, and X. Y. Kuang, J. Mol. Model. **18**, 3061 (2012).
[32] P. Shao, X. Y. Kuang, L. P. Ding, M. M. Zhong, and Z. H. Wang, Physica B **407**, 4379 (2012).
[33] H. F. Li, X. Y. Kuang, and H. Q. Wang, Phys. Lett. A **375**, 2836 (2011).
[34] G. D. Zhou and L. Y. Duan, Structural Chemistry Basis, Peking University Press, Beijing 2002.